Key Points:
- We find stronger temperature trends on nonrainy days compared to rainy days in observations from China
- The reason is likely to be the different sensitivity of downwelling longwave radiation to greenhouse gases on nonrainy and rainy days
- Our findings are consistent with the stronger temperature trends in drier regions because of fewer rainy days

Correspondence to:
A. Kleidon and F. Sun,
axel.kleidon@bgc-jena.mpg.de;
sunfb@igsnrr.ac.cn

Stronger Global Warming on Nonrainy Days in Observations From China

Muye Du[1,2,3] [ID], **Axel Kleidon**[2] [ID], **Fubao Sun**[1,3,4,5,6] [ID], **Maik Renner**[2] [ID], and **Wenbin Liu**[1] [ID]

[1]Key Laboratory of Water Cycle and Related Land Surface Processes, Institute of Geographic Science and Natural Resources Research, Chinese Academy of Sciences, Beijing, China, [2]Max-Planck-Institute for Biogeochemistry, Jena, Germany, [3]College of Resources and Environment, University of Chinese Academy of Sciences, Beijing, China, [4]State Key Laboratory of Desert and Oasis Ecology, Xinjiang Institute of Ecology and Geography, Chinese Academy of Sciences, Urumqi, China, [5]Akesu National Station of Observation and Research for Oasis Agro-ecosystem, Akesu, China, [6]Center for Water Resources Research, Chinese Academy of Sciences, Beijing, China

Abstract Nonrainy days have rather different hydrologic and radiative conditions than rainy days, but few investigations considered how these different conditions contribute to the observed global warming. Here, we show that global warming is considerably stronger on nonrainy days using observations from China. We find that trends in mean temperature on nonrainy days are about 0.1 ° C/10 yr higher than on rainy days, and that about 80% of the total temperature increase is contributed by nonrainy days. The main reason is likely to be a stronger sensitivity of downwelling longwave radiation to greenhouse forcing on nonrainy days due to fewer clouds and water vapor compared with rainy days, which is not a hydrological effect but mainly a radiative effect. Our findings are consistent with the stronger mean temperature trends in drier regions and imply that the different temperature sensitivities on nonrainy and rainy days may have profound effects on natural and social systems.

1. Introduction

Nonrainy and rainy days are two distinct types of days with rather different hydrological conditions. On nonrainy days, evapotranspiration removes water from the soil and adds it to the atmosphere, while the opposite takes place on rainy days. The radiative conditions are also different since typically there are fewer clouds on nonrainy days, enhancing solar radiation at the surface during the daytime and lowering downwelling longwave radiation compared to rainy days (Camberlin, 2016; A. Dai et al., 1997). As a result, the diurnal temperature range on nonrainy days is typically higher with a higher maximum temperature during the day and a lower minimum temperature during night (A. Dai et al., 1999; Stephens et al., 2012; Sun et al., 2000). With these distinct differences in hydrological and radiative conditions, one may expect different manifestations of global warming on nonrainy and rainy days.

Global warming, the increase in near-surface temperature due to the enhanced greenhouse effect at global scale, has clearly been reflected in observations over the last 50 years (Brown & Caldeira, 2017; Easterling, 1997; Fischer & Knutti, 2015; Ji et al., 2014; Piao et al., 2010), impacting the natural and social systems (W. Liu, Lim, et al., 2018; W. Liu, Sun, et al., 2018; Lobell et al., 2011; Trenberth, 2011; C. Zhou & Wang, 2017). Temperature trends vary significantly among different regions and seasons (Cohen et al., 2012; J. Huang et al., 2012; James et al., 2017; Morice et al., 2012). Although several factors, such as adjustments in the atmospheric circulation, land surface-atmosphere interactions, and snow cover changes, were considered to contribute to global warming, the underlying mechanisms have not been clearly identified (Choi et al., 2018; S. Dai et al., 2016; Davy et al., 2017; Guan et al., 2015; Guo et al., 2018; Y. Zhang et al., 2017; L. Zhou, 2016). In previous studies, temperature trends have been decomposed into trends in daytime and nighttime temperatures (Davy et al., 2017), in different seasons (Choi et al., 2018), in different regions (James et al., 2017; Morice et al., 2012), and in different periods (Ji et al., 2014). Here, we focus on how global warming manifests itself on nonrainy and rainy days, an aspect that would be important for the effects of global warming on agriculture and ecology. Moreover, if different temperature trends on nonrainy and rainy days were detected, it would lead to a peculiar pattern of global warming due to the uneven distribution of precipitation frequency, which would contribute to the observed pattern of global warming, and would also affect the occurrence of extreme events such as droughts and heatwaves.

To analyze this difference in trends, we used daily observations of air temperature and precipitation from meteorological stations in China to calculate temperature trends on nonrainy and rainy days separately. In the last 50 years, near-surface temperatures in China showed clear trends with simultaneous and significant changes in precipitation (Chen et al., 2018; Jianping Huang et al., 2017; W. Liu & Sun, 2019; Piao et al., 2010; A. Wang & Zeng, 2011; R. Zhang, 2017). We decomposed the total temperature trends into trends on nonrainy and rainy days using a weighted-average framework. We then evaluated the likely reasons for a different response from the perspective of the surface energy balance using the same data sets to keep it consistent with our results. We describe the data and methodology in the next section, present our results, discuss the likely reasons for the differences in trends and their implications. We close with a brief summary and conclusions.

2. Data and Method

2.1. Data

We used daily (20:00–20:00 local time) precipitation, air temperature, and relative humidity observations for the period 1951–2017 from the *Dataset of Daily Climate Data from Chinese Surface Stations (V3.0)* consisting of 839 meteorological stations (Figure 1a) with daily observations. These data have been quality-controlled by the China Meteorological Data Service Center (CMDC, http://data.cma.cn/) before being released to the scientific community. To have a consistent sample size of stations with continuous and long records, we selected the years 1966–2017 as the time period considered here with 659 stations remaining. From these stations, we first discarded 140 stations with discontinuous precipitation records, because we cannot determine rainy and nonrainy days from those records. We then discarded 63 stations with missing temperature observations on more than two consecutive days. One station was discarded with more than 10% of the values missing for relative humidity in a single year. For stations with missing data of temperature and humidity that were not discarded we filled the gaps by linear interpolation. We also discarded 38 stations which changed the locations with a corresponding significant break point in observations according to the meta data document and the SNHT test (Alexandersson & Moberg, 1997).

The selection of continuous records resulted in a total of 455 stations distributed in both arid and humid regions across China, which cover a wide range of climatological conditions. To show this, the spatial pattern of the radiative dryness index surrounding the stations is presented in Figure 1b. The radiative dryness index is the ratio of net radiation to the latent heat of precipitation, which was proposed by Budyko (Budyko, 1974). We calculate this index from the ratio of potential evapotranspiration to precipitation, with potential evapotranspiration estimated by the Hargreaves equation from the temperature observations (Hargreaves & Samani, 1985).

For the classification of nonrainy and rainy days, we regard days with precipitation less than 0.1 mm as nonrainy days and the effects of fog, dew, and frost were neglected. This is different from the definition in some of the previous studies, which defines a nonrainy day by precipitation being less than 1 mm (Agnese et al., 2014; Frich et al., 2002; Q. Zhang et al., 2011). The reason that we used a less stringent criterion here is to get a sufficiently large sample size of rainy days in arid regions. We also tested the stricter criterion, which led to similar results, but resulted in less spatial coverage.

Since precipitation frequency and temperature both have seasonal patterns in China, we removed the climatological seasonal variation in temperature before the analysis to simplify the results. To do this, we first calculated the multiannual mean for each day of the year using 11-day moving averages to obtain a climatological seasonal variation for each station. We then subtracted this variation from the original data series to derive the anomalies. We also performed the analysis with seasonal means (i.e., without removing the seasonal variation) and found similar results (not shown).

2.2. Decomposition of Temperature Trends

We used a weighted-average framework to evaluate the contributions of temperature trends on nonrainy and rainy days to total temperature trends. First, mean characteristics $(\overline{T})$ for daily mean temperature (Tmean), diurnal temperature range (DTR), minimum temperature (Tmin), and maximum temperature (Tmax) are calculated as the arithmetic mean of daily observations. This could also be expressed as the weighted average of mean temperature characteristics of rainy $(\overline{T}_r)$ and nonrainy days $(\overline{T}_n)$:
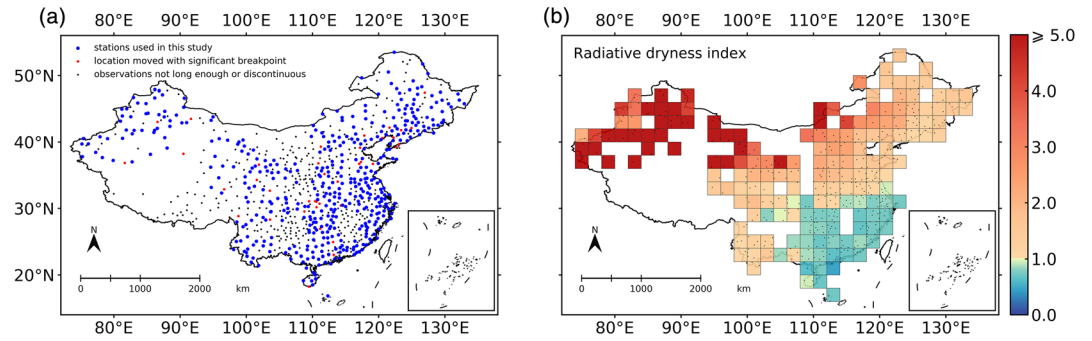
Figure 1. Spatial distribution of 839 meteorological stations in China. (a) The spatial distribution of stations used in this study (blue dots), stations with location moved (red dots) and stations with too short or discontinuous observations (black dots). (b) The radiative dryness index aggregated to a 2 ° × 2° grid. The aggregation was done by averaging the values of the stations used in the study and that are located within the respective grid cell.

$$\overline{T} = \lambda \cdot \overline{T}_r + (1 - \lambda) \cdot \overline{T}_n \tag{1}$$

where λ represents precipitation frequency (assumed to be equal to the frequency of rainy days).

With global warming, we assume each variable in equation 1 changes by a certain amount. The total change $\Delta \overline{T}$ then results from the contributions of temperature changes on nonrainy days, $\Delta \overline{T}_n$, rainy days, $\Delta \overline{T}_r$, as well as a change in the frequency of rainy days $\Delta \lambda$:

$$\Delta \overline{T} = (1 - \lambda) \cdot \Delta \overline{T}_n + \lambda \cdot \Delta \overline{T}_r + \Delta \lambda \cdot \left(\overline{T}_r - \overline{T}_n + \Delta \overline{T}_r - \Delta \overline{T}_n \right) \tag{2}$$

The change in temperature is thus composed of three terms: The first two terms, $(1 - \lambda) \cdot \Delta \overline{T}_n$ and $\lambda \cdot \Delta \overline{T}_r$, represent the contributions by the changes taking place on nonrainy and rainy days, respectively, while the third term, $\Delta \lambda \cdot \left(\overline{T}_r - \overline{T}_n + \Delta \overline{T}_r - \Delta \overline{T}_n \right)$, represents the contribution due to changes in the frequency of rainy days.

We calculated annual means, anomalies as well as the linear trends for each variable in equation 1. The linear trends are obtained by ordinary least squares (OLS). Based on this, we then quantify the contributions of nonrainy and rainy days to total temperature trends using equation 2.

3. Results

3.1. Temperature Characteristics on Nonrainy and Rainy Days

We first evaluated the differences in mean temperature characteristics on nonrainy and rainy days to show that these differences are consistent with differences in radiative conditions (Figure 2a, Table 1). Most stations show higher mean temperature (with a median difference of +1.29 ° C), a greater diurnal temperature range (with a median difference of +3.81 ° C), lower minimum temperatures (with a median difference of −0.73 ° C), and higher maximum temperatures (with a median difference of +2.88 ° C) on nonrainy days than on rainy days. These differences are consistent with what would be expected due to the higher solar radiation and lower greenhouse forcing on nonrainy days caused by fewer clouds. Cloud radiative effects therefore appear to be a crucial part in the relationship between precipitation and temperature.

3.2. Temperature Trends on Nonrainy and Rainy Days

We next calculated the temperature trends using all days as well as nonrainy and rainy days separately (Figure 3, with statistics shown in Table 1). We found that at most stations, temperature characteristics on nonrainy days respond generally more strongly than those on rainy days. Specifically, temperatures generally warm about 0.1 ° C/10 yr more strongly on nonrainy days than on rainy days, which is about 27–50% of the temperature trends on rainy days. The trends in diurnal temperature range are more concentrated around zero for rainy days, while they show a larger spread for nonrainy days (Table 1, Figures 2b and 2c).
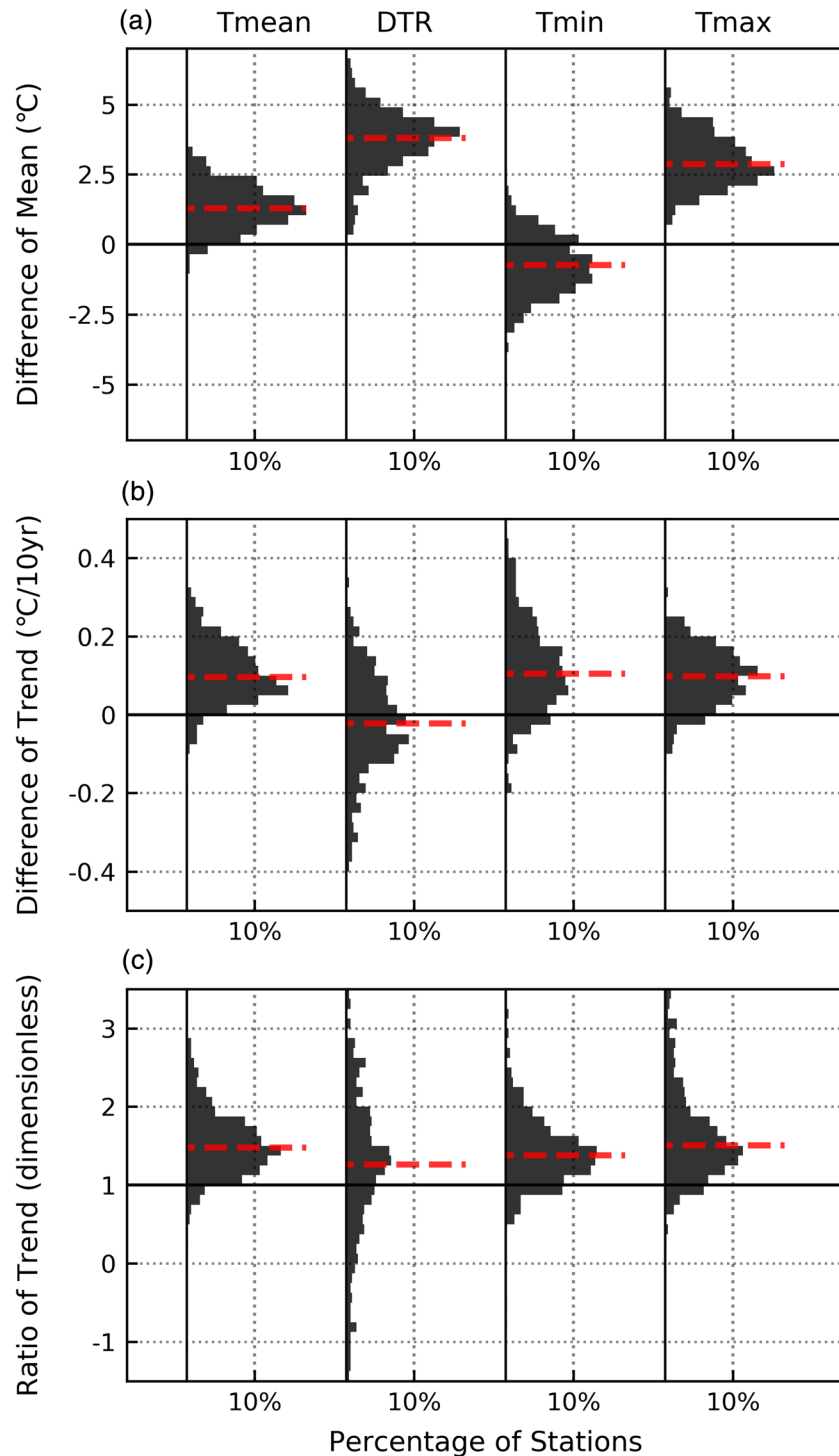
Figure 2. Differences in temperature characteristics between nonrainy and rainy days. The histograms show the differences in (a) mean values and (b) trends as well as (c) the ratio of trends on nonrainy and rainy days for 455 meteorological stations in China. Red dashed lines represent the median values.

3.3. Decomposition of Temperature Trends

We then quantified the contribution of nonrainy days to the overall temperature trends in which the trend is decomposed into the contributions by nonrainy days, rainy days, and the change in frequency of rainy days.

Table 1
Median and Interquartile Range (in Brackets) for Temperature Characteristics and Trends on Nonrainy (Index n) and Rainy (Index r) Days

	Tmean	DTR	Tmin	Tmax
$\overline{T}_n - \overline{T}_r$ (°C)	1.29 (1.08)	3.81 (1.25)	−0.73 (1.51)	2.88 (1.35)
$\overline{T}$ (°C/10yr)	0.30 (0.14)	−0.11 (0.23)	0.37 (0.22)	0.25 (0.14)
$\Delta\overline{T}_n$ (°C/10yr)	0.32 (0.16)	−0.13 (0.26)	0.42 (0.25)	0.28 (0.16)
$\Delta\overline{T}_r$ (°C/10yr)	0.21 (0.12)	−0.11 (0.13)	0.29 (0.14)	0.17 (0.14)
$\Delta\overline{T}_n - \Delta\overline{T}_r$ (°C/10yr)	0.10 (0.11)	−0.02 (0.17)	0.11 (0.15)	0.10 (0.11)
$\Delta\overline{T}_n / \Delta\overline{T}_r$ (dimensionless)	1.48 (0.54)	1.26 (1.49)	1.38 (0.50)	1.51 (0.73)

We find that the mean temperature trends are mostly shaped by the trends in nonrainy days (Table 2, Figure 4). The temperature increases on nonrainy days account for most part of the total trend (76–86% in the median), while rainy days only account for a small part (19–24% in the median). The effect of changes
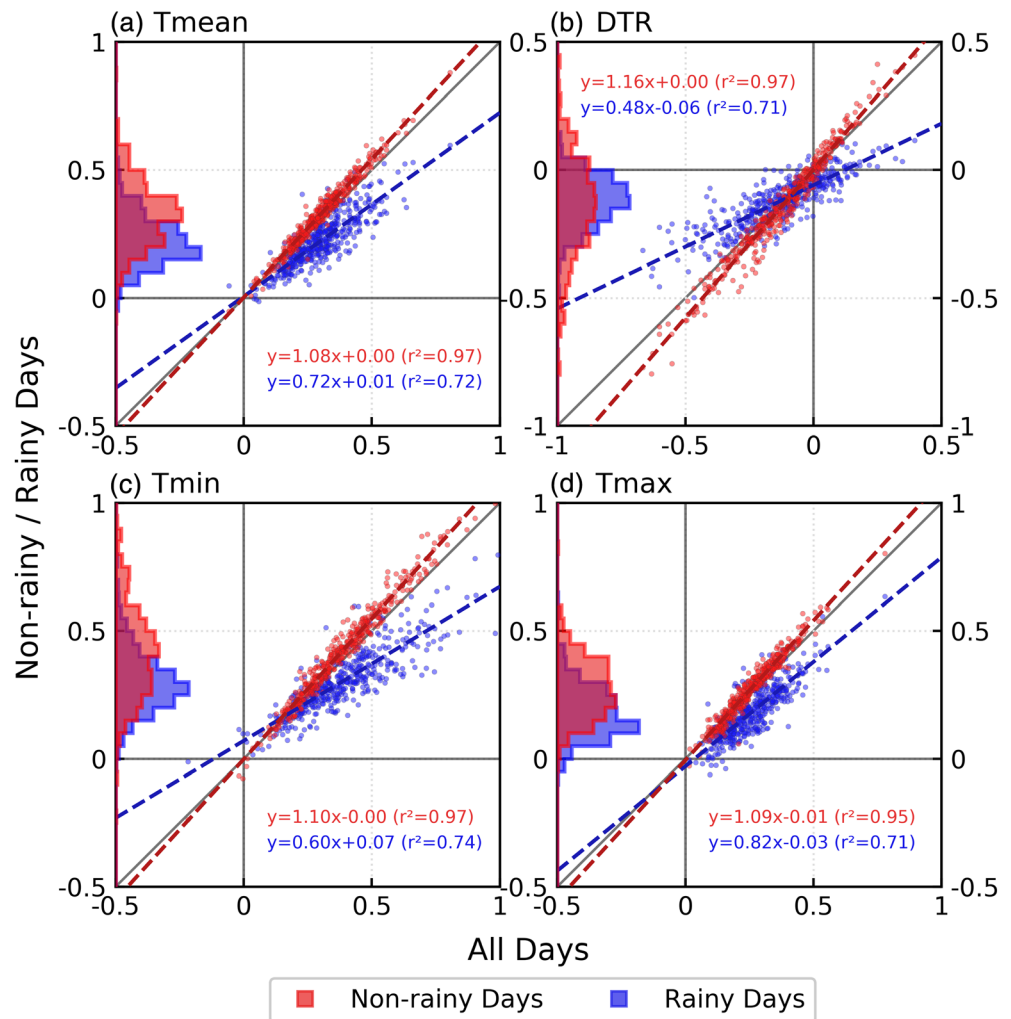

Figure 3. Temperature trends on nonrainy (red) and rainy (blue) days against trends on all days in °C/10 yr. (a) Daily mean temperature; (b) diurnal temperature range; (c) minimum temperature; (d) maximum temperature. Histograms represent the distributions of temperature trends.

Table 2

Median and Interquartile Range (in Brackets) for the Contributions of Nonrainy and Rainy Days and the Change in Precipitation Frequency (λ, Assumed to be Equal to the Frequency of Rainy Days) to Total Temperature Trends (see Equation 2)

	Tmean	DTR	Tmin	Tmax
$(1-\lambda)\cdot\Delta\overline{T}_n$	76% (18%)	86% (22%)	76% (17%)	76% (20%)
$\lambda\cdot\Delta\overline{T}_r$	22% (15%)	19% (27%)	24% (18%)	20% (15%)
$\Delta\lambda\cdot\left(\overline{T}_r-\overline{T}_n+\Delta\overline{T}_r-\Delta\overline{T}_n\right)$	1% (4%)	−4% (22%)	−0.3% (2%)	4% (8%)

in the frequency of rainy days is small, contributing −3–4% in the median. This disproportionally large contribution by nonrainy days to the overall temperature trend is caused by the combination of the higher frequency of nonrainy days (1 − λ, about 69% in the median) and the stronger temperature increases on nonrainy days ($\Delta\overline{T}_n$).
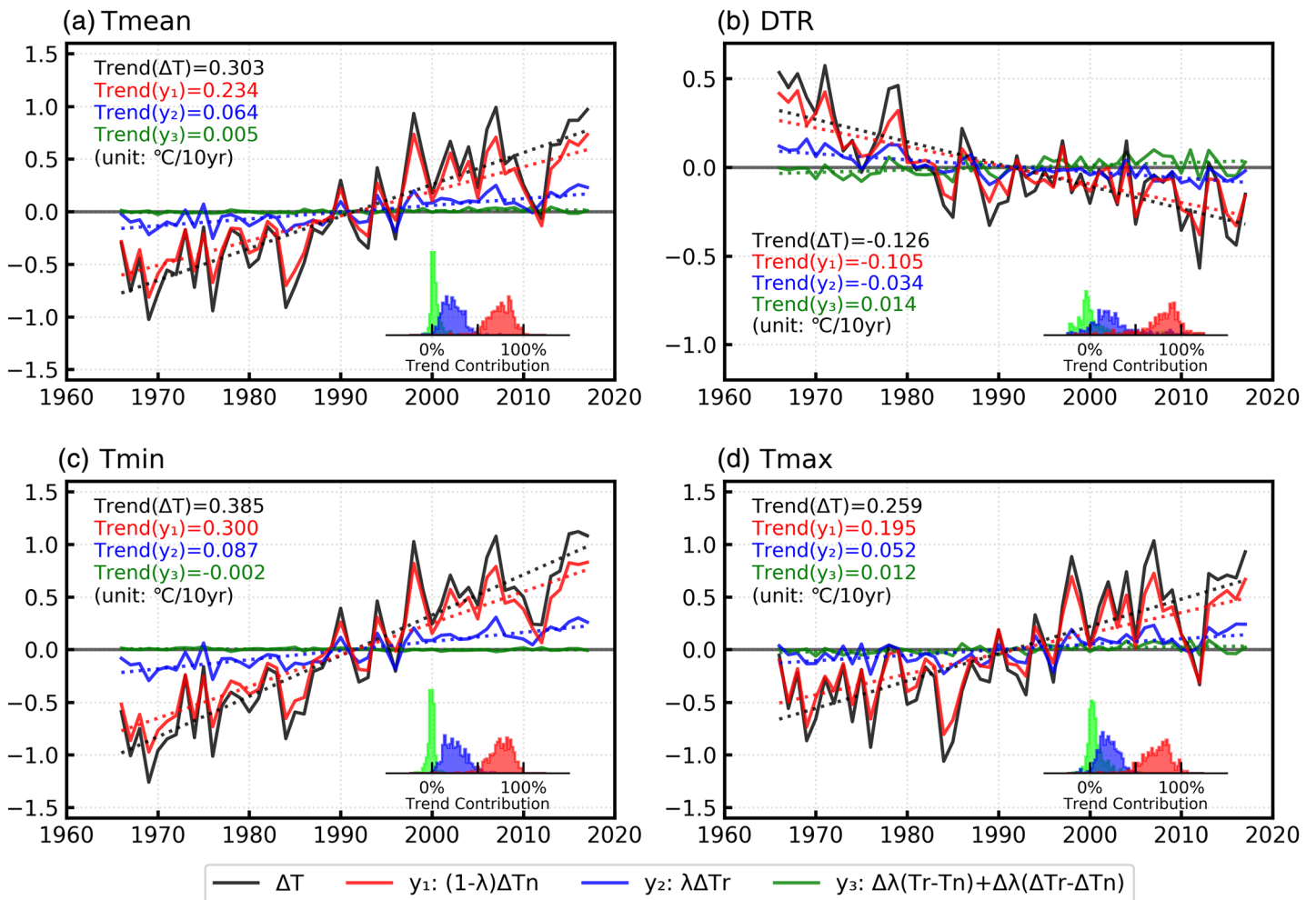

Figure 4. Decomposition of temperature trends to the warming on nonrainy days (red), rainy days (blue) as well as the changes in frequency of rainy days (green) for (a) daily mean temperature; (b) diurnal temperature range; (c) minimum temperature; (d) maximum temperature. Histograms represent the distributions of the contributions of three parts to the total temperature trends.

4. Discussion

To provide a plausible interpretation for these different temperature trends, we analyzed the changes in the surface energy balance. We considered three factors, shortwave radiation, evapotranspiration, and longwave radiation, which could have changed, to analyze whether they show different trends on nonrainy and rainy days.

If the trends of surface solar radiation due to global dimming, brightening, or changes in precipitation intensity (Zhai et al., 2005; C. Zhou & Wang, 2017) were higher on nonrainy days than on rainy days, it could result in stronger mean temperature trends, but also in higher trends in the diurnal temperature range on nonrainy days than on rainy days. However, we find that for many stations the trends in the diurnal temperature range on nonrainy days is lower (see Figure 2b and Table 1). This suggests that a different trend in solar radiation on nonrainy and rainy days is unlikely to be the primary cause for these differences in temperature trends.

If changes in precipitation intensity altered evaporation differently on nonrainy and rainy days, it could also impact temperature trends. This change in evaporation would depend on water availability and radiative conditions, which would affect the differences in temperature trends differently in arid regions, where evaporation is limited by precipitation, and humid regions, where evaporation is limited by net radiation. However, we did not find such consistent differences across regions (Figure 5). Thus, the evaporative cooling effect cannot be the main cause for the different temperature trends neither.

As the third possible cause we looked at changes in downwelling longwave radiation, R_{ld}. It is well known that global warming is mainly caused by the increase in R_{ld} due to the increase in concentrations of greenhouse gases and the water vapor feedback (Held & Soden, 2000; IPCC, 2014; Philipona et al., 2005). Therefore, if R_{ld} increases more strongly on nonrainy days than rainy days, it could lead to a stronger temperature trend on nonrainy days. Since long-term observations for longwave radiation do not exist over the length of the meteorological records used here, we use a commonly used semiempirical parameterization (Crawford & Duchon, 1999; K. Wang & Liang, 2009) to estimate R_{ld}, which we then use to evaluate possible trends in R_{ld}. The first step is to determine downwelling longwave radiation for clear-sky conditions, R_{ldc}:

$$R_{ldc} = \varepsilon_c \sigma T_a^4 \tag{3}$$

where $\varepsilon_c \leq 1$ is the clear-sky atmospheric emissivity which is generally determined by the concentration of greenhouse gases in the atmosphere (Brutsaert, 1975), σ represents the Stefan-Boltzmann constant, and T_a is the near-surface air temperature (unit: K). Since the well-known greenhouse effect of clouds, it is important to correct it with cloud fraction f when estimating R_{ld} (Crawford & Duchon, 1999; K. Wang & Liang, 2009):

$$R_{ld} = f \sigma T_a^4 + (1-f) R_{ldc} \tag{4}$$

The cloud fraction f can be obtained from solar fluxes at the surface by (Crawford & Duchon, 1999; K. Wang & Liang, 2009):

$$f = 1 - R_{sd}/R_{sdc} \tag{5}$$

where R_{sd} is the downwelling flux of solar radiation at the surface and R_{sdc} is the equivalent flux under clear-sky conditions.

With the increase in concentrations of greenhouse gases as well as the water vapor feedback, ε_c in equation 3 increases, thus R_{ldc} as well as R_{ld} increase, which heat the surface more strongly, resulting in warmer temperatures. On the one hand, cloud fraction f is generally lower on nonrainy days than rainy days, which would enhance the increase of R_{ld} on nonrainy days according to equation 4. On the other hand, ε_c could also behave differently on nonrainy and rainy days. We can estimate such a change in ε_c using absolute humidity ρ_v (unit: g/m^3) derived from station data according to a semiempirical approach (Brutsaert, 1975):

$$\varepsilon_c = 1.24(e/T_a)^{1/7} = 1.24(\rho_v R_v)^{1/7} \tag{6}$$

where e is water vapor pressure (unit: hPa) and R_v is the ideal gas constant of water vapor. Combining
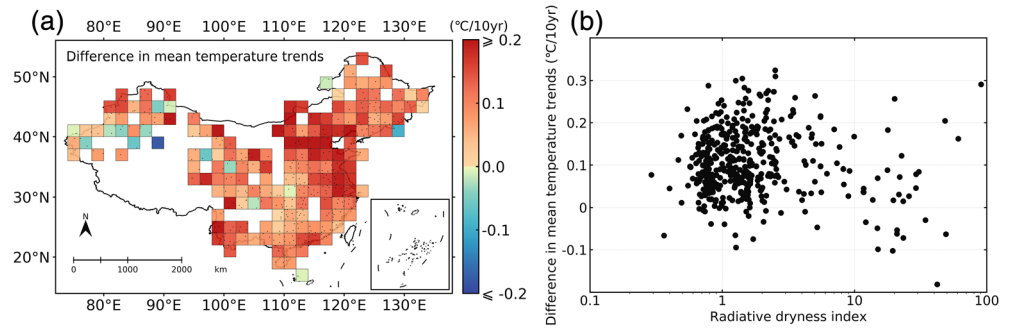
Figure 5. (a) Spatial distribution of differences between mean temperature trends on nonrainy and rainy days $(\overline{T}_n - \overline{T}_r)$, aggregated to a 2° × 2° grid and (b) its relationship with the radiative dryness index.

equations 3–6, this stronger sensitivity in R_{ld} on nonrainy days can be seen by taking the derivative of R_{ld} to ρ_v,

$$\frac{dR_{ld}}{d\rho_v} = \frac{1.24 R_v^{1/7}}{7} \rho_v^{-6/7} (1-f)\sigma T_a^4 \tag{7}$$

which shows clearly that the sensitivity of R_{ld} to ρ_v decreases with cloud fraction f and ρ_v. Considering that nonrainy days typically have lower f and ρ_v than rainy days, it is reasonable for R_{ld} to increase more strongly on nonrainy days. Using observations of relative humidity to derive absolute humidity, we found that rainy days have higher values than nonrainy days (12.68 g/m³ vs. 8.83 g/m³, Table 3), although they have similar trends in ρ_v on nonrainy and rainy days (both around +0.07g/m³/10 yr in their median).

To support this line of reasoning further, we looked at how downwelling longwave radiation has likely changed if only water vapor increases according to equation 6 using median values obtained from observations (shown in Table 3). Since cloud cover is not included in the observations, we used the ERA5 reanalysis (C3S, 2017) to estimate the average cloud fraction on nonrainy and rainy days over China. To do this, we extracted the mean value using daily data on land for the region that covers China [73°E,136°E,3°N,54°N] for the time period 1980–2017 and took the median values for all grid cells. Noticing that gridded data would significantly enlarge the frequency of rainy days, the real difference of cloud fraction between nonrainy and rainy days could be larger than what we show here.

With the values shown in Table 3, we estimated the differences in trends of R_{ld} on nonrainy and rainy days to be ≈0.13 W m⁻²/10 yr, which is considerable compared to the global mean strength of the water vapor feedback of ≈1.5 W m⁻² K⁻¹ (R. Liu, Su, et al., 2018). Therefore, even if greenhouse gases increase the same amount on nonrainy and rainy days, downwelling longwave radiation would react more strongly on nonrainy days since the mean greenhouse effect on nonrainy days is much lower than that on rainy days. It is thus reasonable for nonrainy days to warm more strongly.

Our interpretation is consistent with the main geographic variation of temperature trends across China (Figure 6a). Given that arid regions with low precipitation frequencies, such as deserts, typically have less water vapor in the atmosphere (Figures 6b, 6c, and 6e), they are likely to have stronger temperature trends, as shown in Figure 6d. This finding is consistent with previous studies that reported stronger temperature trends in regions with less precipitation (Portmann et al., 2009; Liming Zhou et al., 2008).

This difference in sensitivities of nonrainy and rainy days may have further implications for interpreting patterns of global warming. As land is typically drier than oceans, it could well be that this effect contributes to the higher climate sensitivity over land than over oceans (Huntingford & Cox, 2000; Kleidon & Renner, 2017; Sutton et al., 2007). This would, however, require a more detailed evaluation of the different sensitivity of longwave downwelling radiation to substantiate the interpretation that we have provided here.
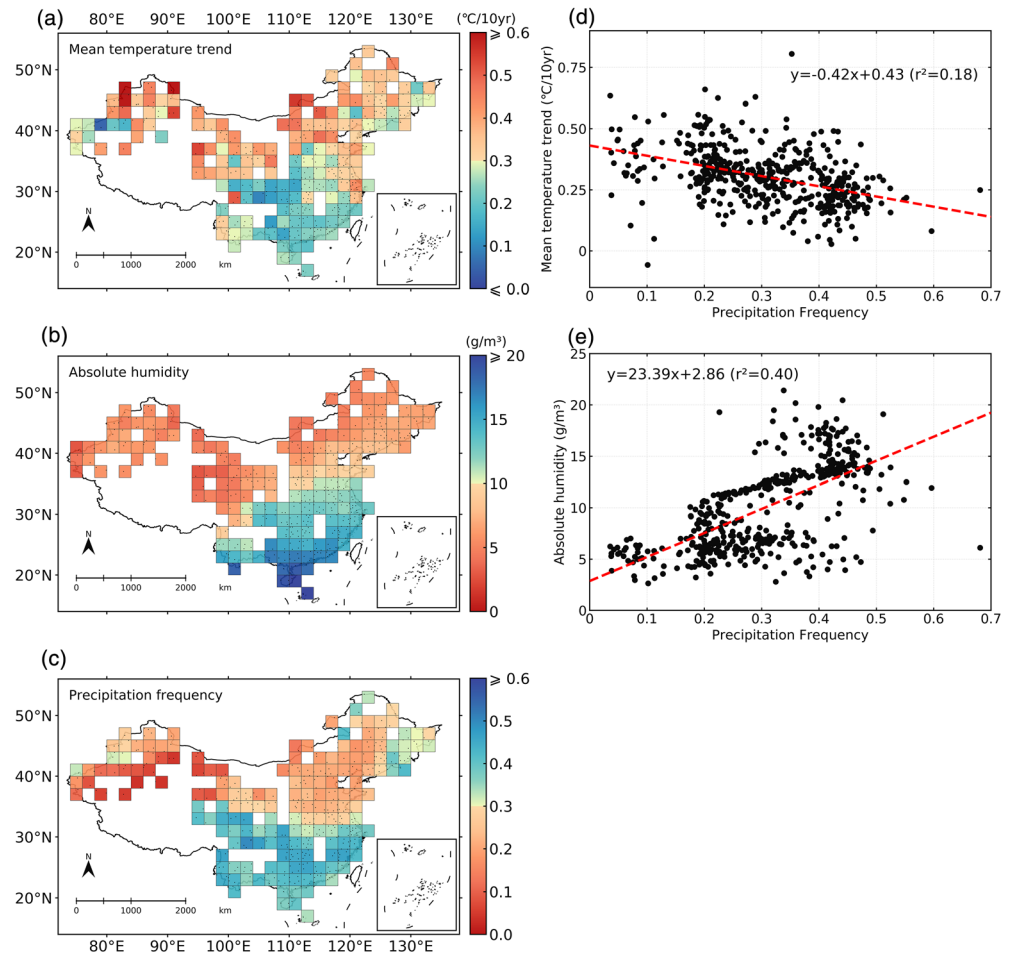
Table 3
Median Values for Equation 7

	Rainy days	Nonrainy days
$d\rho_v/dt$	+0.07 g/m³/10 yr	+0.07 g/m³/10 yr
ρ_v	12.68 g/m³	8.83 g/m³
f	0.30	0.07
σT_a^4	396.0 W m⁻²	380.5 W m⁻²

Figure 6. Spatial distribution of (a) mean temperature trends, (b) absolute humidity, and (c) precipitation frequency (each 2 ° × 2° grid cell presents the average value of the stations contained in); and relationships between precipitation frequency and (d) mean temperature trends (e) absolute humidity.

5. Conclusions

Using observations from meteorological stations, we found that the temperature trends on nonrainy days are distinctly higher than those on rainy days in China and that most of the observed temperature increase is contributed by nonrainy days. We attributed this difference to the higher sensitivity of downwelling long-wave radiation on nonrainy days because of fewer clouds and water vapor. Our findings are consistent with previous studies showing stronger temperature increases in more arid regions.

Our findings identify an indirect connection between hydrologic cycling and global warming in that regions with less precipitation frequency also typically have fewer clouds and less water vapor and thus warm more strongly. This is, however, not a hydrologic effect, but rather likely due to different sensitivities of radiative effects. What our results imply is that the stronger temperature trends on nonrainy days is significant and may play an important role in amplifying the temperature response during extreme events, such as heat waves and droughts.

References

Agnese, C., Baiamonte, G., & Cammalleri, C. (2014). Modelling the occurrence of rainy days under a typical Mediterranean climate. *Advances in Water Resources*, *64*, 62–76.

Alexandersson, H., & Moberg, A. (1997). Homogenization of Swedish temperature data. Part I: Homogeneity test for linear trends. *International Journal of Climatology*, *17*(1), 25–34.

Brown, P. T., & Caldeira, K. (2017). Greater future global warming inferred from Earth's recent energy budget. *Nature*, *552*(7683), 45–50.

Brutsaert, W. (1975). On a derivable formula for long-wave radiation from clear skies. *Water Resources Research*, *11*(5), 742–744.

Budyko, M. I. (1974). *Climate and life*. New York: Academic Press.

Camberlin, P. (2016). Temperature trends and variability in the greater horn of Africa: Interactions with precipitation. *Climate Dynamics*, *48*(1–2), 477–498.

Chen, J., Liu, Y., Pan, T., Liu, Y., Sun, F., & Ge, Q. (2018). Population exposure to droughts in China under the 1.5 °C global warming target. *Earth System Dynamics*, *9*(3), 1097–1106.

Choi, W., Ho, C.-H., Kim, M.-K., Kim, J., Yoo, H.-D., Jhun, J.-G., & Jeong, J.-H. (2018). Season-dependent warming characteristics observed at 12 stations in South Korea over the recent 100 years. *International Journal of Climatology*, *38*(11), 4092–4101.

Cohen, J. L., Furtado, J. C., Barlow, M., Alexeev, V. A., & Cherry, J. E. (2012). Asymmetric seasonal temperature trends. *Geophysical Research Letters*, *39*, L04705. https://doi.org/10.1029/2011gl050582

Copernicus Climate Change Service (C3S). (2017). *ERA5: Fifth generation of ECMWF Atmospheric reanalyses of the global climate*, Copernicus Climate Change Service Climate Data Store (CDS): https://cds.climate.copernicus.eu/cdsapp#!/home

Crawford, T. M., & Duchon, C. E. (1999). An improved parameterization for estimating effective atmospheric emissivity for use in calculating daytime downwelling longwave radiation. *Journal of Applied Meteorology*, *38*(4), 474–480.

Dai, A., Genio, A. D. D., & Fung, I. Y. (1997). Clouds, precipitation and temperature range. *Nature*, *386*(6626), 665–666.

Dai, A., Trenberth, K. E., & Karl, T. R. (1999). Effects of clouds, soil moisture, precipitation, and water vapor on diurnal temperature range. *Journal of Climate*, *12*(8), 2451–2473.

Dai, S., Shulski, M. D., Hubbard, K. G., & Takle, E. S. (2016). A spatiotemporal analysis of Midwest US temperature and precipitation trends during the growing season from 1980 to 2013. *International Journal of Climatology*, *36*(1), 517–525.

Davy, R., Esau, I., Chernokulsky, A., Outten, S., & Zilitinkevich, S. (2017). Diurnal asymmetry to the observed global warming. *International Journal of Climatology*, *37*(1), 79–93.

Easterling, D. R. (1997). Maximum and minimum temperature trends for the globe. *Science*, *277*(5324), 364–367.

Fischer, E. M., & Knutti, R. (2015). Anthropogenic contribution to global occurrence of heavy-precipitation and high-temperature extremes. *Nature Climate Change*, *5*(6), 560–564.

Frich, P., Alexander, L. V., Della-Marta, P., Gleason, B., Haylock, M., Klein Tank, A. M. G., & Peterson, T. (2002). Observed coherent changes in climatic extremes during the second half of the twentieth century. *Climate Research*, *19*, 193–212.

Guan, X., Huang, J., Guo, R., Yu, H., Lin, P., & Zhang, Y. (2015). Role of radiatively forced temperature changes in enhanced semi-arid warming in the cold season over east Asia. *Atmospheric Chemistry and Physics*, *15*(23), 13,777–13,786.

Guo, R., Guan, X., He, Y., Gan, Z., & Jin, H. (2018). Different roles of dynamic and thermodynamic effects in enhanced semi-arid warming. *International Journal of Climatology*, *38*(1), 13–22.

Hargreaves, H. G., & Samani, Z. A. (1985). Reference crop evapotranspiration from temperature. *Applied Engineering in Agriculture*, *1*(2), 96–99.

Held, I. M., & Soden, B. J. (2000). Water vapor feedback and global warming. *Annual Review of Energy and the Environment*, *25*(1), 441–475.

Huang, J., Guan, X., & Ji, F. (2012). Enhanced cold-season warming in semi-arid regions. *Atmospheric Chemistry and Physics*, *12*(12), 5391–5398.

Huang, J., Yu, H., Dai, A., Wei, Y., & Kang, L. (2017). Drylands face potential threat under 2 °C global warming target. *Nature Climate Change*, *7*(6), 417–422.

Huntingford, C., & Cox, P. M. (2000). An analogue model to derive additional climate change scenarios from existing GCM simulations. *Climate Dynamics*, *16*(8), 575–586.

IPCC (2014). *Climate Change 2013: The physical science basis*. Cambridge: Cambridge Univ Press.

James, R., Washington, R., Schleussner, C.-F., Rogelj, J., & Conway, D. (2017). Characterizing half-a-degree difference: A review of methods for identifying regional climate responses to global warming targets. *Wiley Interdisciplinary Reviews: Climate Change*, *8*(2).

Ji, F., Wu, Z., Huang, J., & Chassignet, E. P. (2014). Evolution of land surface air temperature trend. *Nature Climate Change*, *4*(6), 462–466.

Kleidon, A., & Renner, M. (2017). An explanation for the different climate sensitivities of land and ocean surfaces based on the diurnal cycle. *Earth System Dynamics*, *8*(3), 849–864.

Liu, R., Su, H., Liou, K. N., Jiang, J. H., Gu, Y., Liu, S. C., & Shiu, C. J. (2018). An assessment of tropospheric water vapor feedback using radiative kernels. *Journal of Geophysical Research: Atmospheres*, *123*(3), 1499–1509.

Liu, W., Lim, W. H., Sun, F., Mitchell, D., Wang, H., Chen, D., et al. (2018). Global freshwater availability below normal conditions and population impact under 1.5 and 2 °C stabilization scenarios. *Geophysical Research Letters*, *45*(18), 9803–9813. https://doi.org/10.1029/2018GL078789

Liu, W., & Sun, F. (2019). Increased adversely-affected population from water shortage below normal conditions in China with anthropogenic warming. *Science Bulletin*, *64*(9), 567–569.

Liu, W., Sun, F., Lim, W. H., Zhang, J., Wang, H., Shiogama, H., & Zhang, Y. (2018). Global drought and severe drought-affected populations in 1.5 and 2 °C warmer worlds. *Earth System Dynamics*, *9*(1), 267–283.

Lobell, D. B., Schlenker, W., & Costa-Roberts, J. (2011). Climate trends and global crop production since 1980. *Science*, *333*(6042), 616–620. https://doi.org/10.1126/science.1204531

Morice, C. P., Kennedy, J. J., Rayner, N. A., & Jones, P. D. (2012). Quantifying uncertainties in global and regional temperature change using an ensemble of observational estimates: The HadCRUT4 data set. *Journal of Geophysical Research, Atmospheres*, *117*, D08101. https://doi.org/10.1029/2011jd017187

Philipona, R., Dürr, B., Ohmura, A., & Ruckstuhl, C. (2005). Anthropogenic greenhouse forcing and strong water vapor feedback increase temperature in Europe. *Geophysical Research Letters*, *32*, L19809. https://doi.org/10.1029/2005gl023624

Piao, S., Ciais, P., Huang, Y., Shen, Z., Peng, S., Li, J., et al. (2010). The impacts of climate change on water resources and agriculture in China. *Nature*, *467*(7311), 43–51. https://doi.org/10.1038/nature09364

Portmann, R. W., Solomon, S., & Hegerl, G. C. (2009). Spatial and seasonal patterns in climate change, temperatures, and precipitation across the United States. *Proceedings of the National Academy of Sciences of the United States of America*, *106*(18), 7324–7329. https://doi.org/10.1073/pnas.0808533106

Stephens, G. L., Li, J., Wild, M., Clayson, C. A., Loeb, N., Kato, S., et al. (2012). An update on Earth's energy balance in light of the latest global observations. *Nature Geoscience*, *5*(10), 691–696. https://doi.org/10.1038/ngeo1580

Sun, B., Groisman, P. Y., Bradley, R. S., & Keimig, F. T. (2000). Temporal changes in the observed relationship between cloud cover and surface air temperature. *Journal of Climate*, *13*(24), 4341–4357.

Sutton, R. T., Dong, B., & Gregory, J. M. (2007). Land/sea warming ratio in response to climate change: IPCC AR4 model results and comparison with observations. *Geophysical Research Letters*, *34*, L02701. https://doi.org/10.1029/2006GL028164

Trenberth, K. E. (2011). Changes in precipitation with climate change. *Climate Research*, *47*(1), 123–138.

Wang, A., & Zeng, X. (2011). Sensitivities of terrestrial water cycle simulations to the variations of precipitation and air temperature in China. *Journal of Geophysical Research*, *116*, D02107. https://doi.org/10.1029/2010jd014659

Wang, K., & Liang, S. (2009). Global atmospheric downward longwave radiation over land surface under all-sky conditions from 1973 to 2008. *Journal of Geophysical Research*, *114*, D19101. https://doi.org/10.1029/2009JD011800

Zhai, P., Zhang, X., Wan, H., & Pan, X. (2005). Trends in total precipitation and frequency of daily precipitation extremes over China. *Journal of Climate*, *18*(7), 1096–1108.

Zhang, Q., Singh, V. P., Li, J., & Chen, X. (2011). Analysis of the periods of maximum consecutive wet days in China. *Journal of Geophysical Research, Atmospheres*, *116*, D23106. https://doi.org/10.1029/2011jd016088

Zhang, R. (2017). Warming boosts air pollution. *Nature Climate Change*, *7*(4), 238–239.

Zhang, Y., Guan, X., Yu, H., Xie, Y., & Jin, H. (2017). Contributions of radiative factors to enhanced dryland warming over East Asia. *Journal of Geophysical Research: Atmospheres*, *122*, 7723–7736.

Zhou, C., & Wang, K. (2017). Quantifying the sensitivity of precipitation to the long-term warming trend and interannual–decadal variation of surface air temperature over China. *Journal of Climate*, *30*(10), 3687–3703.

Zhou, L. (2016). Desert amplification in a warming climate. *Scientific Reports*, *6*(1), 31,065. https://doi.org/10.1038/srep31065

Zhou, L., Dai, A., Dai, Y., Vose, R. S., Zou, C.-Z., Tian, Y., & Chen, H. (2008). Spatial dependence of diurnal temperature range trends on precipitation from 1950 to 2004. *Climate Dynamics*, *32*(2–3), 429–440.